Comparative study on the densification of chromium pre-alloyed powder metallurgy steel through nanopowder addition using design of experiments

Downloaded from: https://research.chalmers.se, 2024-04-19 13:48 UTC

Citation for the original published paper (version of record):
Manchili, S., Wendel, J., Vattur Sundaram, M. et al (2021). Comparative study on the densification of chromium pre-alloyed powder metallurgy steel through
nanopowder addition using design of experiments. Results in Materials, 10.
http://dx.doi.org/10.1016/j.rinma.2021.100173

N.B. When citing this work, cite the original published paper.

research.chalmers.se offers the possibility of retrieving research publications produced at Chalmers University of Technology.
It covers all kind of research output: articles, dissertations, conference papers, reports etc. since 2004.
research.chalmers.se is administrated and maintained by Chalmers Library

(article starts on next page)

Results in Materials 10 (2021) 100173

Contents lists available at ScienceDirect

Results in Materials

journal homepage: www.journals.elsevier.com/results-in-materials

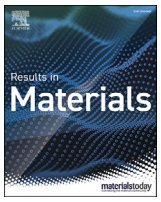

Comparative study on the densification of chromium pre-alloyed powder metallurgy steel through nanopowder addition using design of experiments

Swathi K. Manchili [a,*], Johan Wendel [a], Maheswaran Vattur Sundaram [b], Eduard Hryha [a], Lars Nyborg [a]

[a] Department of Industrial and Materials Science, Chalmers University of Technology, Gothenburg, SE-41296, Sweden
[b] Högänas AB, Högänas, SE-26383, Sweden

ARTICLE INFO

Keywords:
Water-atomized steel powder
Dilatometry
Nanopowder
Thermal analysis

ABSTRACT

There is a constant demand for high density press and sinter powder metallurgical components for automotive applications. Steel powder pre-alloyed with chromium is an attractive material for such applications, but new ways to further increase the sinter density are required for successful processing of these powders to high density. Nanopowder could be used as a potential sintering aid in order to boost the densification of the steel powder compact. In this study, steel powder pre-alloyed with chromium, without and with admixed nickel, is used as base powder, to which nanopowder was added. Surface oxide removal, crucial for successful sintering of such materials, was studied by thermogravimetry analysis in order to understand the influence of nanopowder addition on the oxide reduction. Powder compacts containing nanopowder showed higher mass loss in comparison to the ones without nanopowder. Linear shrinkage obtained from dilatometric curves increased with the addition of nanopowder. To depict the influence of the critical parameters; sintering temperature, powder size, addition of nanopowder and composition (with or without nickel), a design of experiment approach was applied. The critical parameters were then adjusted at 2 different values (categorical parameters) and a 'full factorial design model' was used involving 16 experiments, with sinter density and hardness as output measures of the experiments determined. The results were analyzed using polynomial fit to determine which of the parameter exerts the maximum influence. Presence of nickel increased the hardness whereas sintering temperature and presence of nanopowder enhanced the sinter density. This led to the tentative design of optimum conditions that resulted in increase in sinter density from 7.25 g/cm^3 (92.5% of the theoretical density) to 7.4 g/cm^3 (94% of the theoretical density) with an addition of 5% nanopowder to Ni-containing grade when sintered at 1350 °C instead of 1250 °C.

1. Introduction

Ferrous powder metallurgy (PM) is a proven technology to manufacture complex shaped products for automotive applications. Among these products, there are PM gears used in different industries as well as in the automotive sector. The PM gears are mostly used for engine parts like sprockets and pulleys, gear shift components, oil pump gears and gears like spur, helical and bevel gears. For large scale production of gears, PM route is preferred over the conventional one as for the lower costs involved, less energy is used and very little material wastage. Compaction and sintering to a final density of 7.5 g/cm^3, which is around 95% of the theoretical density of steel, is achievable for a certain kind of gears [1]. Mechanical properties have a direct correlation with the porosity of the component. As the density increases more than 95% of the theoretical density, mechanical properties increase significantly [2–5]. Hence, there is a constant drive to further improve the density in order to use PM process for high performance applications.

There are different ways of improving the density of PM components like increasing the compaction pressure, applying so-called warm compaction or increasing the sintering temperature. Increasing compaction pressure adversely affects the compaction die involving higher tool wear, while increasing sintering temperature requires use of high temperature sintering furnaces, which may not necessarily be desirable for an industrial set up. Another way of improving the density is to use an additive that helps improving the sinter density, without a need to increase the compaction pressure or sintering temperature. Addition of nanopowder is one of the ways to increase the sinter density. Powder with particle sizes in the order of 1–100 nm are referred to as

* Corresponding author.
E-mail address: manchili@chalmers.se (S.K. Manchili).

https://doi.org/10.1016/j.rinma.2021.100173
Received in revised form 9 December 2020; Accepted 29 December 2020
Available online 24 January 2021
2590-048X/© 2021 The Authors. Published by Elsevier B.V. This is an open access article under the CC BY license (http://creativecommons.org/licenses/by/4.0/).

Table 1
Experimental conditions of two-level factorial design.

Factor/variables	Levels	
	−1	+1
Sintering temperature, °C	1250	1350
Particle size, μm	<45	SF (20–180 μm)
Iron nanopowder (Fe NP)	Without Fe NP	With Fe NP
Composition	Without Ni	With Ni

nanopowder [6]. The small diameter of the nanopowder is associated with large surface area that increases the excess surface energy and lowers the sintering temperature and hence decrease the activation energy for sintering [7,8]. Nanopowder is prone to explosive oxidation and the high price associated with it makes it challenging to apply nanopowder in PM processing route [9]. Nanopowder can be added in small proportions to the normal micrometer-sized steel powder making micro/nano bimodal powder compact to tap the advantages of the potential sintering aid effect, while limiting the aforementioned disadvantages. The authors have explored the addition of iron nanopowder as a sintering aid to water-atomized iron powder [10]. The sinter curves revealed pronounced influence of nanopowder addition on the sintering behavior. At temperatures as low as 500 °C, the compact containing nanopowder showed densification and the fractographic analysis of the sintered compacts were in agreement with the observations from sinter curve.

The objective of the larger framework of research, of which this investigation is a part, is to be able to achieve full density in PM components produced through press and sinter route based on water atomized steel powder. While complete densification of powder is not new and is achieved through hot isostatic pressing (HIP) after encapsulation of the powder, it can only be used for low volume high cost products [11]. A combination of cost and energy efficient press and sinter route producing near net shapes when combined with full densification using capsule-free HIP could open up possibilities for PM steel to be used in highly demanding applications [12].

The current study is intended primarily to evaluate if the previous work by the authors performed on densification in pure iron nano-micro powder system stands valid for commercial water atomized alloy systems used in high performance applications. In this study, the addition of iron nanopowder has been applied to chromium-alloyed steel powder without and with admixed nickel. Alloying elements are added and mixed in the form of elemental powder in order to maintain a high level of compressibility. Fully pre-alloyed powder has high hardness and reduced compressibility. In the present case, nickel, in the form of fine powder, is added to the chromium pre-alloyed powder and is mixed. To study only the effect of the nanopowder itself, the normal addition of carbon was avoided and hence the result can thus not yet depict any technological or industrial practice. The aim was hence to analyze the readiness level of the addition of nanopowder approach for further development towards industrial practice. Design of experiments was therefore used for identifying the most pertinent factors that affect the sinter density and hardness of the powder compacts. A 'full factorial design' was preferred as the approach was reliable based on a mathematical model of the combined effect of the processing factors [13].

2. Materials

2.1. Materials

Two different grades of water atomized steel powder, supplied by Höganäs AB, were studied. The first one was a grade pre-alloyed with 1.8 wt % Cr, while the other one also contained 2 wt % admixed nickel. Henceforth, the first powder would be known as CrA while the second one as CrA+Ni. Two different particle size distributions were considered; <45 μm and standard fraction 20–180 μm (SF) for both the powder variants. Pure iron nanopowder with size below 100 nm procured from Sigma Aldrich was added to the water-atomized steel powder as a sintering aid. Mixing of the powder was carried out using a tumbler placed in a glovebox.

2.2. Design of experiments

A full factorial design was used in order to evaluate the effect of the four factors as shown in Table 1 on the observed responses (sinter density and hardness). The JMP 7 software (from SAS institute at Cary, NC, USA) was applied for analysis of the results. As the factors chosen were categorical, two alternative levels are ascribed to each of the four factors whose experimental values are as follows: 1) sintering temperature being 1250 or 1350 °C, 2) particle size distribution being SF or <45 μm, 3) powder mix without or with 5 wt% of iron nanopowder and 4) base powder composition without or with 2 wt% added nickel. In total, 16 sintering experiments (2^4) were conducted according to this experimental design as listed in Table 2.

For each of the trails, sinter density and hardness were determined.

3. Methods

3.1. Dilatometry

Powder was compacted using a uniaxial compaction press at 600 MPa which yielded in cylindrical samples of the size 10 mm diameter and 2 mm height. The compacts were sintered at 1250 and 1350 °C using a DIL 402C horizontal push rod dilatometer (Netzsch Thermal Analysis GmbH,

Table 2
Experimental details.

Trail no.	Sintering temperature, °C	Size, base powder, μm	Composition	Fe nanopowder	Sample
1	1350	20–180	Without Ni	Without Fe NP	CrA, SF
2	1250	<45	Without Ni	With Fe NP	CrA+Fe NP, −45
3	1350	<45	With Ni	With Fe NP	CrA+Ni+Fe NP, −45
4	1250	<45	With Ni	Without Fe NP	CrA+Ni, −45
5	1250	20–180	With Ni	With Fe NP	CrA+Ni+Fe NP, SF
6	1250	20–180	Without Ni	Without Fe NP	CrA, SF
7	1350	20–180	Without Ni	With Fe NP	CrA+Fe NP, SF
8	1250	20–180	With Ni	Without Fe NP	CrA+Ni, SF
9	1350	<45	With Ni	Without Fe NP	CrA+Ni, −45
10	1350	20–180	With Ni	With Fe NP	CrA+Ni+Fe NP, SF
11	1250	20–180	Without Ni	With Fe NP	CrA+Fe NP, SF
12	1350	20–180	With Ni	Without Fe NP	CrA+Ni, SF
13	1250	<45	With Ni	With Fe NP	CrA+Ni+Fe NP, −45
14	1350	<45	Without Ni	Without Fe NP	CrA, −45
15	1250	<45	Without Ni	Without Fe NP	CrA, −45
16	1350	<45	Without Ni	With Fe NP	CrA+Fe NP, −45

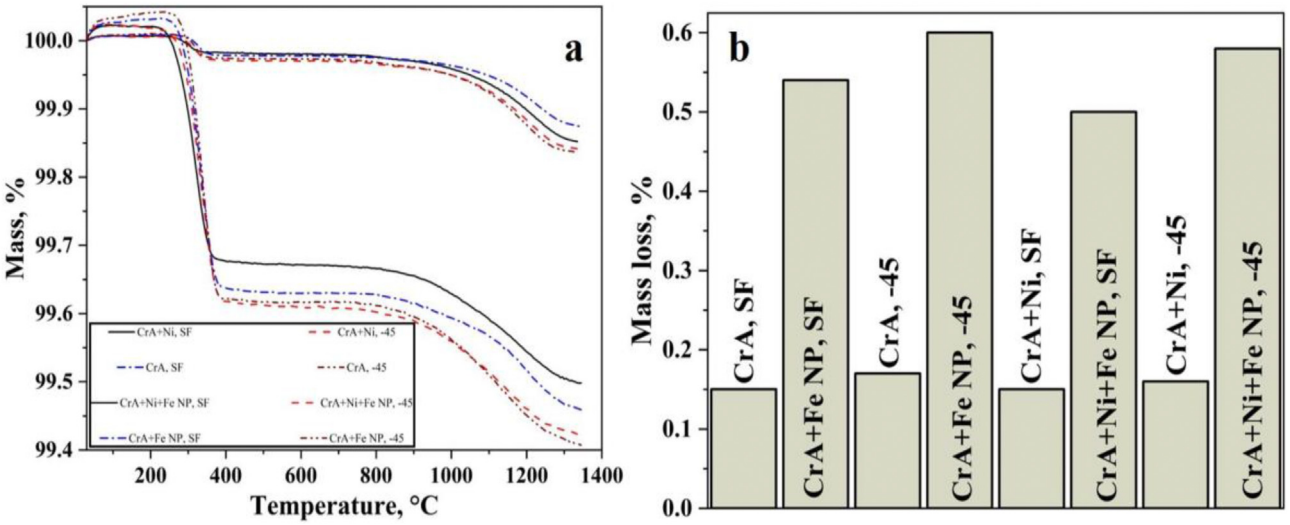

Fig. 1. (a) Thermogravimetric curves for CrA+Ni SF, CrA+Ni −45 μm, CrA SF, CrA −45 μm, CrA+Ni+Fe NP SF, CrA+Ni+Fe NP -45 μm, CrA+Fe NP SF and CrA+Fe NP -45 μm powder heated to 1350 °C at a heating rate of 10 °C/min in pure hydrogen atmosphere. (b) Mass loss, in percentage, recorded for different powder combinations using thermogravimetry measured in pure hydrogen atmosphere when heated to 1350 °C.

Germany). Sintering was carried out in pure hydrogen atmosphere at a heating rate of 10 °C/min, held at peak sintering temperature for 30 min and cooled to room temperature at 30 °C/min. The sintering temperature 1250 °C is used in industrial set up for the sintering of ferrous powder when improved sinter density and mechanical performance are needed. One sample per condition was sintered. Samples were also sintered at 1350 °C to understand the high temperature sintering behavior. Pure hydrogen atmosphere (99.9999% purity) was used for all the sintering experiments and a flow rate of 100 ml/min was employed.

3.2. Thermal analysis

Thermogravimetric (TG) measurements were carried out using a simultaneous thermal analyzer STA 449 F1 Jupiter equipment (Netzsch Thermal Analysis GmbH, Germany). Powder of required mass was loaded into an alumina crucible and heated to 1350 °C at a heating rate of 10 °C/min followed by cooling at 30 °C/min from the peak sintering temperature. Three different samples were evaluated for TG. Pure hydrogen atmosphere of same quality as dilatometry studies was used at a flow rate of 100 ml/min for all the experiments. Pure hydrogen was used in order to maximize the reduction of surface oxides at low temperatures. In previous works by the authors [14] it was shown that the oxide scale on the nanopowder reduces before 500 °C. Similarly, it was also shown that the oxide scale on the water-atomized steel powder reduces at low temperatures in the presence of hydrogen [15]. It is known that the reduction of surface oxide promotes sintering and hydrogen being an effective reducing agent at low temperatures, hydrogen was chosen as the atmosphere.

3.3. Density

Green density of the compacts was evaluated using a micrometer and a simple balance with an accuracy of 0.0001 g. The micrometer was used to measure the height and the diameter of the cylinder to calculate the volume of the compact. The simple balance was used to measure the mass of the compact. Density of the sintered compacts was measured using two different methods: Archimedes principle and image analysis using metallographic cross-sections. Porosity was measured from optical micrographs taken at different locations using image analysis software. Area fraction of the porosity was measured from 20 different micrographs taken per sample.

3.4. Hardness

The apparent hardness testing was performed using Struers DuraScan 70G5 (Ballerup, Denmark) Vickers hardness tester at 1 kg load on metallographic cross-sections of sintered compacts.

4. Results and discussion

4.1. Thermogravimetry

The different variants of powder were subjected for thermogravimetric (TG) analysis. Mass loss by the powder in hydrogen environment is recorded as a function of temperature. Powder variants without nanopowder showed smaller mass loss than the variant with nanopowder addition (Fig. 1a). The details of mass loss values for each powder are shown in Fig. 1b. For the powder without nanopowder, the mass loss was approximately 3–4 times lower when compared to the powder with nanopowder. The <45 μm CrA powder when combined with nanopowder showed the highest mass loss of 0.60% up to 1350 °C followed by the variant <45 μm CrA+Ni+Fe NP with slightly lowered mass loss of 0.58%. The SF variants CrA+Fe NP and CrA+Ni+Fe NP showed mass losses of 0.54 and 0.50%, respectively. For the powder without nanopowder the mass loss values ranged from 0.15 to 0.17%.

The TG curve could be divided into two parts. The first part, in the temperature range below 400 °C, the surface oxide film of the base powder as well as of the nanopowder is reduced. For both kinds of powder, the oxide consists of Fe oxide. The second temperature range, from 800 °C and upwards, depicts the reduction of particulate oxides, that are present to minor extent on the surfaces of the base powder, as well as internal oxides [15].

The mass loss of the powder is hence a result of the reduction of surface and particulate oxides present on the powder surface as well as internal oxides. As the particle size is reduced, the surface area of the powder increases. Though the thickness of the surface oxide is the same for both −45 and SF powder [16], the increased surface area increases the mass loss for the powder with −45 μm size fraction in comparison to that of SF powder. Furthermore, the nanopowder is associated with much higher specific surface area and as said the metal nanopowder is invariably covered with a surface oxide scale, but lacks presence of particulate oxides [14]. Therefore, the increased mass loss of the first region below 400 °C for the samples with nanopowder can be explained in terms of the high specific surface area, and hence higher amount of

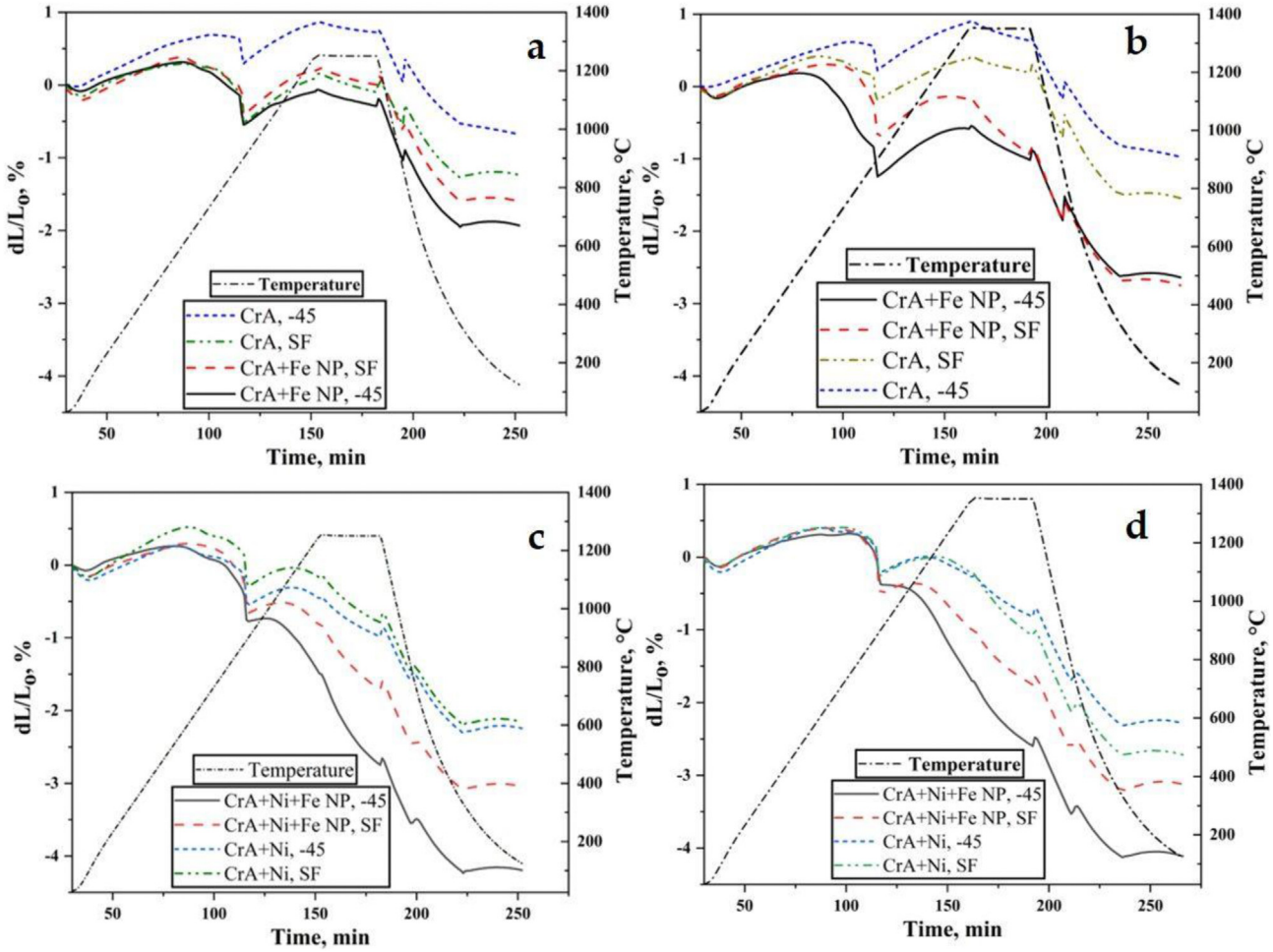

Fig. 2. Sinter curves showing the linear shrinkage for compacts sintered in pure hydrogen environment in a dilatometer (a) CrA -45 μm, CrA SF, CrA+Fe NP -45 μm and CrA+Fe NP SF at 1250 °C, (b) CrA -45 μm, CrA SF, CrA+Fe NP -45 μm and CrA+Fe NP SF at 1350 °C, (c) CrA+Ni -45 μm, CrA+Ni SF, CrA+Ni+Fe NP -45 μm and CrA+Ni+Fe NP SF at 1250 °C and (d) CrA+Ni -45 μm, CrA+Ni SF, CrA+Ni+Fe NP -45 μm and CrA+Ni+Fe NP SF at 1350 °C.

surface oxide, associated with nanopowder. The reduction temperature of the oxide scale is strongly dependent on composition of powder. CrA powder is covered by an oxide scale, predominantly an iron-based oxide, but is reduced at temperatures lower than that of pure iron powder oxide surface [15]. Finer particle sizes also have lower reduction temperature for surface oxides layer in comparison to the coarser size fractions and this is believed to be due to increase in surface area in finer fractions [16].

4.2. Sintering

Compacted green body when heated to high temperature, below the melting point of base metal, leads to the formation metallurgical bonds between the particles is called sintering. These metallurgical bonds formed at the necks between the particles provide the strength to the compact. The compacts were subjected to sintering in dilatometer. Fig. 2 shows the sintering curves of the compacts when heated at 10 °C/min up to the two target sintering temperatures employed. All the compacts were otherwise sintered under identical conditions. The change in the linear dimension of the compact is measured as a function of time and temperature and the curve is divided into 3 different stages. During the heating stage of the sintering, the material has to expand, and the slope of the curve gives the coefficient of thermal expansion. In addition, there can be further sintering taking place during the heating stage which can be identified from earlier onset of sintering than at the target sintering temperature employed. During the isothermal holding stage, the compact undergoes shrinkage and during the cooling stage, the compact is expected to thermally shrink. Phase transformation from BCC ferrite (alpha) to FCC austenite (gamma), generally observed in iron systems, is also be expected to be seen in the sinter curves.

Fig. 2 shows the sinter curves for all the specimens under study. Fig. 2a and b shows the sinter curves for CrA compacts, for two different size fractions, with and without nanopowder, sintered at 1250 °C and 1350 °C respectively. For the compacts containing powder, of two size fractions, along with 2 wt % Ni, sinter curves for the compacts sintered at 1250 °C with and without nanopowder are shown in Fig. 2c, while the compacts sintered at 1350 °C are shown in Fig. 2d.

When comparing the data in the Fig. 2, it is clear that the compacts with nanopowder showed consistently higher linear shrinkage compared to the ones without such addition. The change in slope of the sinter curves during heating as well as cooling around 900 °C could be explained through the phase transformation undergone. It was observed at 900 °C for the CrA compacts whereas at 906 °C for compacts containing the nanopowder. The transformation temperature decreased to 890 °C in compacts with Ni, since Ni is an austenite stabilizer. When nanopowder was added it changed to 900 °C. Addition of nanopowder changes the overall alloy composition and this change reflects on the phase transformation temperature.

The shrinkage increased slightly when employing a higher target sintering temperature; for example, the total shrinkage was changed from 1.5 to 1.6% for SF CrA compact. Also, when the particle size was reduced to <45 μm, the shrinkage was 0.6% for 1250 °C, while was 1.0% for 1350 °C. The addition of nanopowder changed the total linear shrinkage to 1.2% and 1.9% for the <45 and the SF variants, respectively, when sintered at 1250 °C, while the shrinkages of 2.7 and 2.6% for the <45 μm and SF variants were found for the sintering at 1350 °C.

The total shrinkage of the CrA+Ni compacts increased from 2.1 to 2.7% for SF size fraction variant when sintering temperature was increased from 1250 °C to 1350 °C. For the <45 μm CrA+Ni compacts, the linear shrinkage increased slightly from 2.2 to 2.3% with increasing sintering temperature from 1250 to 1350 °C. For the compacts with added nanopowder, shrinkage increased from 3.0 to 3.1% for the SF variant of CrA+Ni compacts when the sintering temperature increased from 1250 to 1350 °C. When the particle size was reduced to <45 μm, shrinkage became 4.1 and 4.2% for sintering at 1250 and 1350 °C, respectively. The shrinkage values for the compacts with Ni were hence higher in comparison to the ones without Ni. The addition of nanopowder resulted in increase in linear shrinkage (Fig. 2). The influence of nanopowder addition has been studied in detail by the authors in another study [10] and the mechanism has been explained through fractographic analysis of compacts sintered at different sintering temperatures from 500 to 1350 °C. It was found that the added nanopowder sintered at temperatures as low as 600 °C which contributed to the linear shrinkage in low temperature regime compared to the compact containing only micrometer-sized iron powder.

The increase in shrinkage for compacts sintered at 1350 °C in comparison to the compacts sintered at 1250 °C was observed in all the cases. The driving force for neck formation and growth is to minimize the free surface energy and it progresses through atomic diffusion mechanisms. Diffusion coefficient depends exponentially on temperature following Arrhenius law. Therefore, the self-diffusion constant of iron at 1250 °C was 8.38 x 10^{10} cm^2/s. As the sintering temperature increases to 1350 °C, the diffusion constant increases to 31.2 x 10^{10} cm^2/s [17].

Nickel is added to the CrA powder through diffusion alloying, where fine nickel powder is bonded to the surface of coarse water atomized steel powder. Through this method, the alloying element attains adequate bonding to the base powder so that the compressibility is retained by limiting the extent of diffusion of alloying element into the base metal. Diffusion of nickel through iron lattice is slow which results in an inhomogeneous composition in sintered parts. Diffusion of nickel along the iron particle surface and its location at the sintering necks has also been reported earlier [18]. Researchers observed that the variation of nickel content resulted in austenite formation in the center of the original nickel particle as the maximum nickel content is left undiffused [19,20]. There have been studies which have shown that the addition of nickel enhances the sintering of iron compacts and the enhancement is a function of quantity of nickel added and depends on the method of addition [21]. This is the case even in the present study, where the compacts containing nickel showed higher shrinkage values in comparison to that of the compacts without nickel.

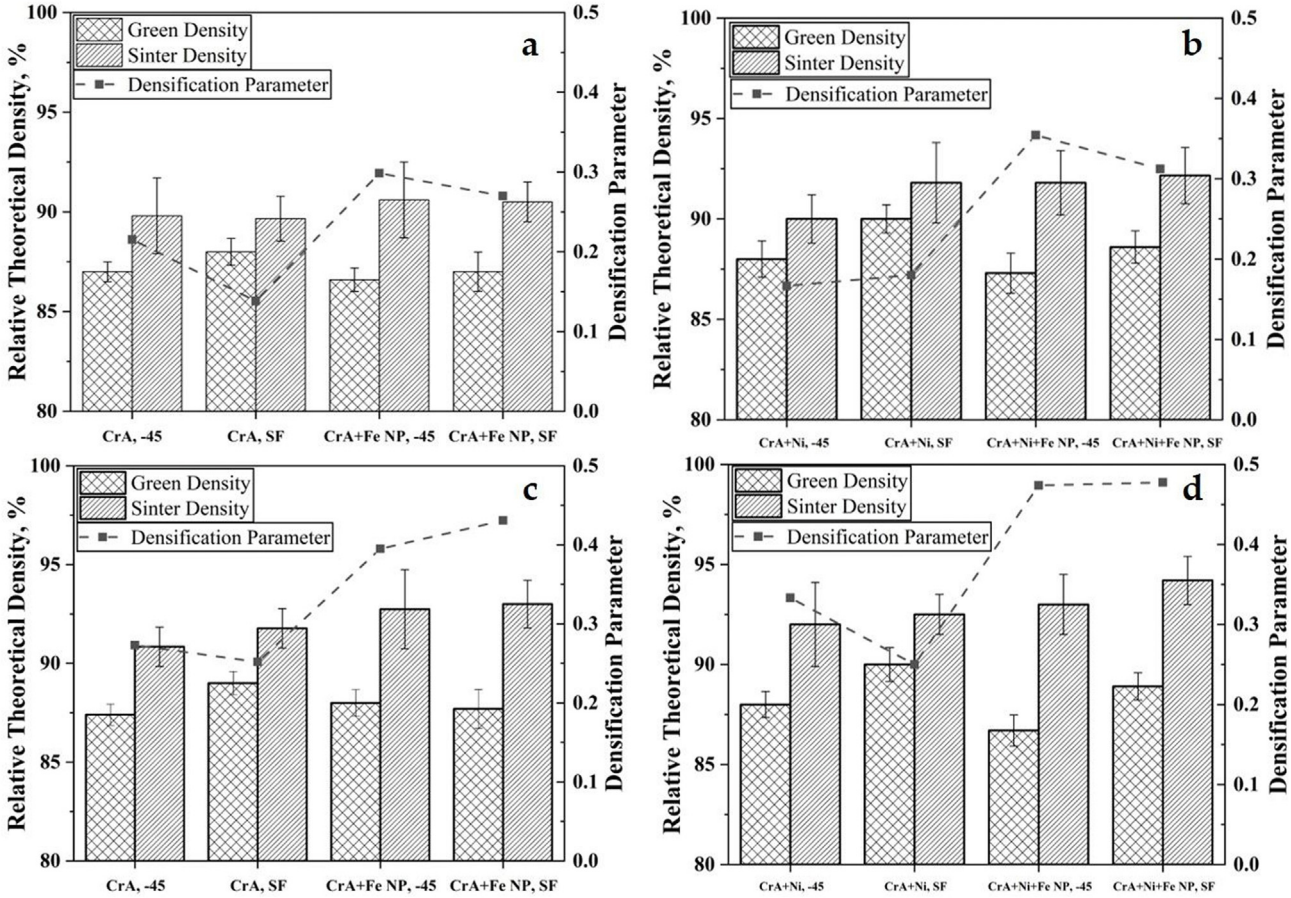

Fig. 3. Plots showing green density and sinter density in terms of relative theoretical density along with densification parameter for compacts sintered at 1250 and 1350 °C in pure hydrogen environment using a dilatometer (a) CrA -45 μm, CrA SF, CrA+Fe NP -45 μm and CrA+Fe NP SF at 1250 °C, (b) CrA+Ni -45 μm, CrA+Ni SF, CrA+Ni+Fe NP -45 μm and CrA+Ni+Fe NP SF at 1250 °C, (c) CrA -45 μm, CrA SF, CrA+Fe NP -45 μm and CrA+Fe NP SF at 1350 °C and (d) CrA+Ni -45 μm, CrA+Ni SF, CrA+Ni+Fe NP -45 μm and CrA+Ni+Fe NP SF at 1350 °C.

Fig. 3(a–d) shows the green and sinter density along with densification parameter for all the compacts. To overcome the challenge in comparing different compacts with varying initial relative densities, densification parameter is used for normalization [22]. Densification parameter, Ψ, is given by the following equation

$$\Psi = \frac{\rho_s - \rho_0}{1 - \rho_0}$$

where ρ_s is the sinter density and ρ_0 is the green density. Densification parameter serves as an indicator for the degree of sintering.

The green density of compacts without nanopowder displayed similar or lower values in comparison to their counterparts without the nanopowder. Lower green density could be attributed to the low compressibility caused by nanopowder addition [10]. The sinter density of compacts with nanopowder was either similar or marginally higher in comparison to the compacts without nanopowder. A clear impact of nanopowder addition was observed through densification parameter. An increase in the value of densification parameter was observed for the compacts with nanopowder in comparison to the compacts without nanopowder. Therefore, it could be said that the addition of nanopowder boosts the degree of sintering. An increase in densification parameter was also observed for the compacts sintered at 1350 °C in comparison to the compacts sintered at 1250 °C. Addition of nickel also increased the degree of sintering.

4.3. Hardness

Fig. 4 shows the hardness plots. The hardness of the compacts sintered at 1350 °C was higher than that of the samples sintered at 1250 °C in all the cases. Fig. 4a shows the hardness values of CrA compacts, sintered at both 1250 and 1350 °C, for both size fractions, with and without iron nanopowder. The hardness for both the compacts, sintered at 1250 and 1350 °C was around 50 HV. Fig. 4b shows the hardness for CrA+Ni compacts. For compacts sintered at 1250 °C, the hardness was around 65 HV for CrA+Ni, −45 μm compact whereas for CrA+Ni, SF it was around 70 HV. In the case of 1350 °C, the hardness was above 70 HV for both −45 μm and SF compacts. The hardness values are lowered for compacts with nanopowder. The addition of alloying elements like Ni, Mo or Cu increases the hardness of as-sintered powder metallurgy steels [23]. Nickel, like Cu, strengthen steels by forming a solid solution with iron. For the compacts with nanopowder, the hardness was marginally lower than the compacts without nanopowder as the overall composition of the alloy is changed due its addition.

4.4. Design of experiments

In the present study, focus was on four factors as listed in Table 1 with two values for each factor. This experimental plan provided an opportunity to analyze the influence of the factors on sinter density and hardness, two separate outputs. The significance of the factor is through the values of Logworth and p-value. A small p-value and larger Logworth value indicate that the factor exerts significant influence on the output [24].

In this case, p-value given by the model is less than 0.0001 for both sinter density and hardness as outputs. Fig. 5 shows the comparative plot between predicted and actual values of the sinter density and hardness. The determination coefficient (RSq=0.87 and RSq=0.97 for sinter density and hardness respectively as seen from Fig. 5b and d) indicates that the model predicts up to 87 and 97% of the total variations. Sintering temperature followed by addition of nanopowder influenced the sinter density (Fig. 5a). Increase in sintering temperature and addition of nanopowder improve the sinter density in press and sinter PM components [25,26]. The size fraction of base powder had the least influence of the four factors. Fig. 5c shows that the composition, addition of nickel, has a dominant effect on the hardness as would be expected. Particle size followed by sintering temperature had low impact on the hardness.

Industrially, sintering temperature is limited to 1250 °C. Keeping sintering temperature constant at 1250 °C, a 'full factorial model' with 3 factors: nanopowder addition, composition (nickel) and size fraction of base powder was used resulting in 8 experiments. Fig. 6 shows that the presence of nanopowder increases the sinter density followed by composition and size.

This study suggests that "closed-porosity", which is achieved at about 95% of the theoretical density levels [27], cannot be achieved under the evaluated conditions and alloy configurations. This could be due to multiple factors like low compaction pressure employed and, low green density of compacts containing nanopowder. However, one important factor which has not been explored and will be a part of the future work is to evaluate effect of carbon which is an essential alloying component in most high-performance PM applications, and has a strong effect on oxide reduction and subsequent sintering enhancement, allowing to decrease porosity level. This will allow to reach components with closed porosity

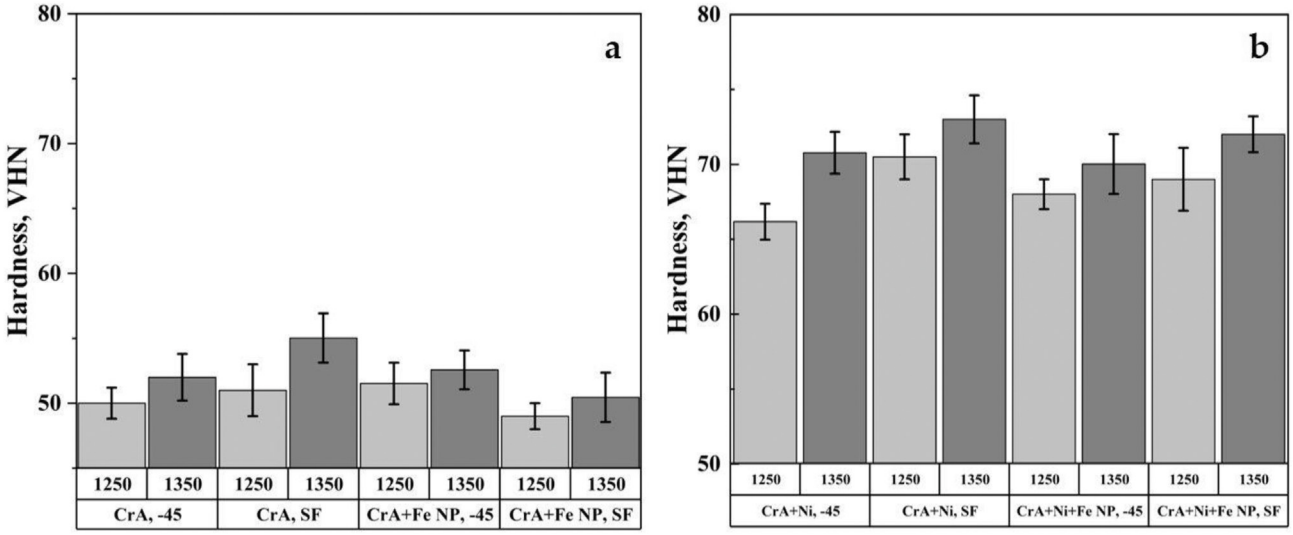

Fig. 4. Plots showing the hardness for the compacts sintered at 1250 and 1350 °C in pure hydrogen atmosphere in a dilatometer (a) CrA -45 μm, CrA SF, CrA+Fe NP -45 μm and CrA+Fe NP SF and (b) CrA+Ni -45 μm, CrA+Ni SF, CrA+Ni+Fe NP -45,mm and CrA+Ni+Fe NP SF.

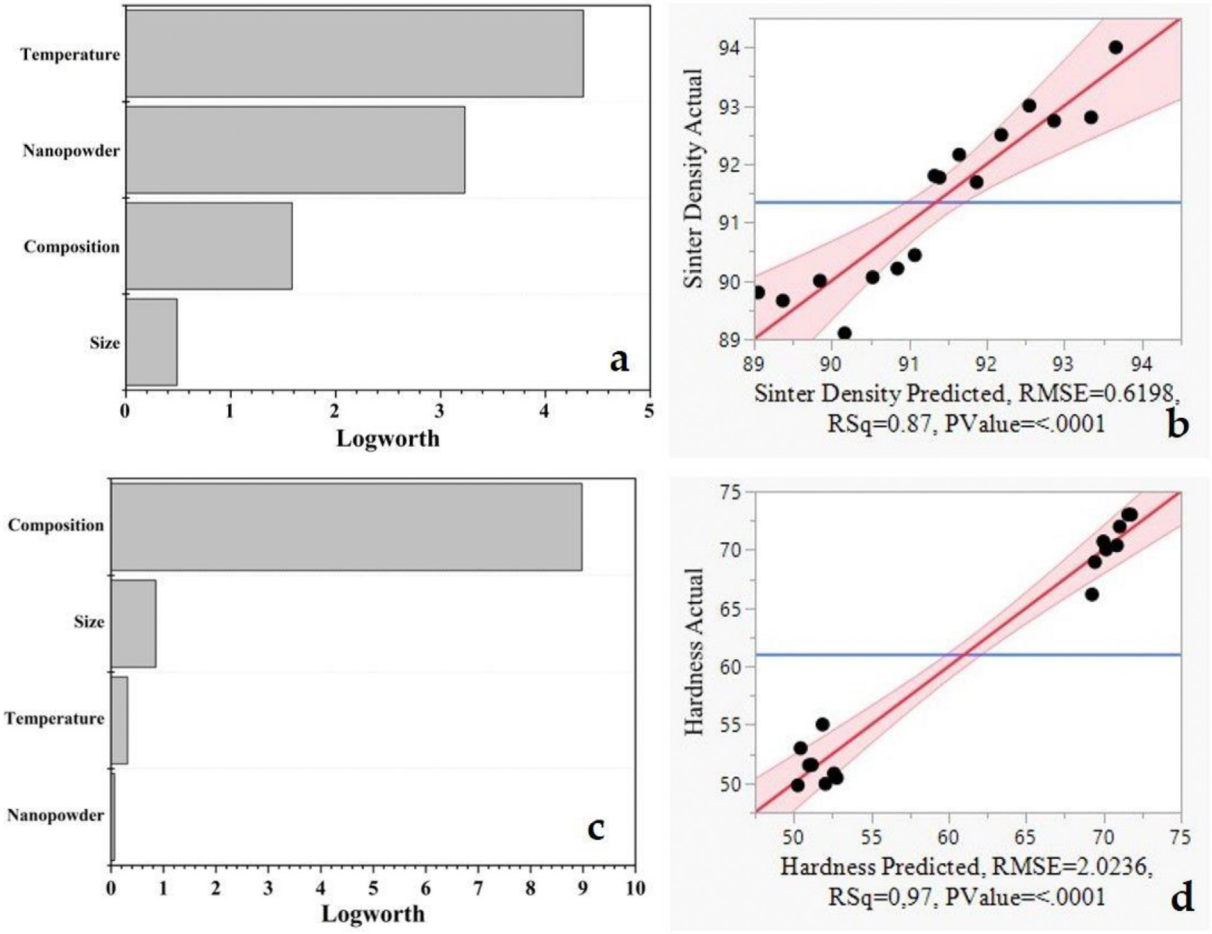

Fig. 5. Design of experiments plots showing (a-b) the influence of different parameters on the sinter density of the compacts sintered at 1250 and 1350 °C in pure hydrogen atmosphere in a dilatometer whereas (c-d) reveal the influence of the same set of parameters on the hardness of the compacts sintered at 1250 and 1350 °C in pure hydrogen atmosphere in a dilatometer.

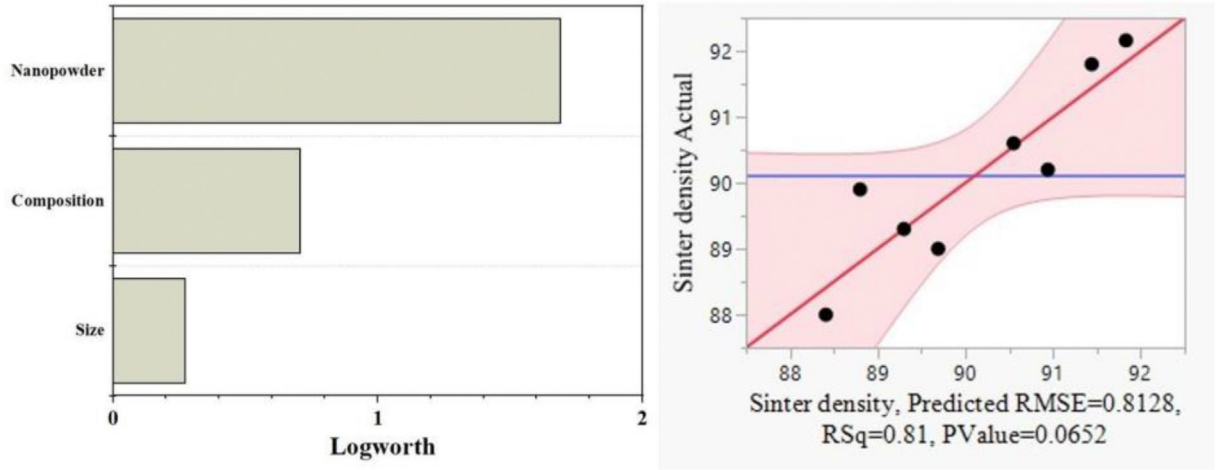

Fig. 6. Design of experiments plots showing the influence of different parameters on the sinter density of the compacts sintered at 1250 °C in pure hydrogen atmosphere in a dilatometer.

and allow further densification by subsequent application of HIP.

5. Conclusions

The present study has illustrated a comparative study of the sintering behavior of steel powder pre-alloyed with chromium, with and without admixed nickel in the presence of nanopowder as sintering aid. Thermogravimetry revealed that the powder containing the nanopowder showed higher mass loss of around 0.60% in comparison to that of the powder without nanopowder of around 0.15%. This additional loss was attributed to surface oxide reduction of nanopowder. Sintering curves revealed that the linear shrinkage increased with addition of

nanopowder, increase in sintering temperature and addition of nickel. Increase in the value of densification parameter value showed that the degree of sintering increased with the addition of nanopowder. Hardness of the sintered compact increased from 50 HV to 70 HV with the addition of nickel. A full factorial model was used to evaluate the influence of the four factors: size of the base powder, composition (nickel), nanopowder addition and sintering temperature (1250 and 1350 °C) on sinter density and hardness. Increase in sintering temperature increased the sinter density followed by nanopowder addition and addition of nickel increased the hardness.

Author contributions

Conceptualization, methodology, investigation, data curation, formal analysis, writing—original draft and visualization, Swathi Manchili.; conceptualization, investigation, and visualization, Johan Wendel.; writing—review, editing, and methodology, Maheswaran Vattur Sundaram; writing-review, editing and supervision, Eduard Hryha; writing—review, editing, supervision, project administration, and funding acquisition, Lars Nyborg. All authors have read and agreed to the published version of the manuscript.

Declaration of competing interest

The authors declare that they have no known competing financial interests or personal relationships that could have appeared to influence the work reported in this paper.

Acknowledgements

This work has been carried out within the project 'Nanotechnology enhanced sintered steel processing' through support from Swedish Foundation for Strategic Research, SSF within the program 'Generic Methods and Tools for Future Production'. The authors would like to acknowledge the support from 'Area of Advance, Production', Chalmers University of Technology. Funding from the strategic innovation program LIGHTer, provided by Vinnova, is also gratefully acknowledged.

References

[1] M. Vattur Sundaram, Novel Approaches for Acheiving Full Density Powder Metallurgy Steels, Chalmers University of Technology, 2019.
[2] Höganäs Handbook for Sintered Components-3. Design and Properties, Höganäs AB, 2004.
[3] W. Xu, X. Lu, B. Zhang, C. Liu, S. Lv, S. Yang, X. Qu, Effects of porosity on mechanical properties and corrosion resistances of PM-fabricated porous Ti-10Mo Alloy, Metals 8 (2018) 1–13, https://doi.org/10.3390/met8030188.
[4] T. Seramak, A. Zielinski, W. Serbinski, K. Zasinska, Powder metallurgy of the porous Ti-13Nb-13Zr alloy of different powder grain size, Mater. Manuf. Process. 34 (2019) 915–920, https://doi.org/10.1080/10426914.2019.1605178.
[5] W. Schatt, K.-P. Wieters, Powder Metallurgy, European Powder Metallurgy Association, Shrwesbury, 1997.
[6] R.W. Siegel, Synthesis and properties of nanophase materials, Mater. Sci. Eng. 168 (1993) 189–197.
[7] K.H. Kim, B.-T. Lee, C.-J. Choi, Fabrication and evaluation of powder injection molded Fe–Ni sintered bodies using nano Fe–50%Ni powder, J. Alloys Compd. 491 (2010) 391–394, https://doi.org/10.1016/j.jallcom.2009.10.192.
[8] J.W. Oh, R. Bollina, W.S. Lee, S.J. Park, Effect of nanopowder ratio in bimodal powder mixture on powder injection molding, Powder Technol. 302 (2016) 168–176, https://doi.org/10.1016/j.powtec.2016.08.051.
[9] J.W. Oh, S.K. Ryu, W.S. Lee, S.J. Park, Analysis of compaction and sintering behavior of 316L stainless steel nano/micro bimodal powder, Powder Technol. 322 (2017) 1–8, https://doi.org/10.1016/j.powtec.2017.08.055.
[10] S.K. Manchili, J. Wendel, A. Zehri, J. Liu, E. Hryha, L. Nyborg, Effect of nanopowder addition on the sintering of water-atomized iron powder, Metall. Mater. Trans. 51 (2020) 4890–4901, https://doi.org/10.1007/s11661-020-05891-1.
[11] P.K. Samal, Introduction to full density powder metallurgy, ASM Handb. Powder Metall., 2018, pp. 253–254, https://doi.org/10.31399/asm.hb.v07.a0006142.
[12] M. Vattur Sundaram, A. Khodaee, M. Andersson, L. Nyborg, A. Melander, Experimental and finite element simulation study of capsule-free hot isostatic pressing of sintered gears, Int. J. Adv. Manuf. Technol. 99 (2018) 1725–1733, https://doi.org/10.1007/s00170-018-2623-4.
[13] Y.-S. Rhee, S.-Y. Chang, C.-W. Park, S.-C. Chi, E.-S. Park, Optimization of ibuprofen gel formulations using experimental design technique for enhanced transdermal penetration, Int. J. Pharm. 364 (2008) 14–20, https://doi.org/10.1016/j.ijpharm.2008.07.029.
[14] S.K. Manchili, R. Shvab, A. Zehri, L. Ye, E. Hryha, J. Liu, L. Nyborg, Surface analysis of iron and steel nanopowder, Surf. Interface Anal. 50 (2018) 1083–1088, https://doi.org/10.1002/sia.6465.
[15] J. Wendel, S.K. Manchili, Y. Cao, E. Hryha, L. Nyborg, Evolution of surface chemistry during sintering of water-atomized iron and low-alloyed steel powder, Surf. Interface Anal. (2020) 1–5, https://doi.org/10.1002/sia.6852.
[16] J. Wendel, R. Shvab, Y. Cao, E. Hryha, L. Nyborg, Surface analysis of fine water-atomized iron powder and sintered material, Surf. Interface Anal. 50 (2018) 1065–1071, https://doi.org/10.1002/sia.6455.
[17] T. Heumann, R. Imm, Self-diffusion and isotope effect in γ-iron, J. Phys. Chem. Solid. 29 (1968) 1613–1621, https://doi.org/10.1016/0022-3697(68)90103-0.
[18] M. Nabeel, Diffusion of Elemental Additives during Sintering, Royal Institute of Technology, 2012.
[19] M.W. Wu, K.S. Hwang, K.H. Chuang, Improved distribution of nickel and carbon in sintered steels through addition of chromium and molybdenum, Powder Metall. 51 (2008) 160–165, https://doi.org/10.1179/174329007X189667.
[20] M.W. Wu, K.S. Hwang, H.S. Huang, In-Situ observations on the fracture mechanism of diffusion-alloyed Ni-containing powder metal steels and a proposed method for tensile strength improvement, Metall. Mater. Trans. A Phys. Metall. Mater. Sci. 38 A (2007) 1598–1607, https://doi.org/10.1007/s11661-007-9201-y.
[21] K.S. Hwang, M.Y. Shiau, Effects of nickel on the sintering behavior of Fe-Ni compacts made from composite and elemental powders, Metall. Mater. Trans. B Process Metall. Mater. Process. Sci. 27 (1996) 203–211, https://doi.org/10.1007/BF02915046.
[22] D.C. Blaine, S.J. Park, P. Suri, R.M. German, Application of work-of-sintering concepts in powder metals, Metall. Mater. Trans. A Phys. Metall. Mater. Sci. 37 (2006) 2827–2835, https://doi.org/10.1007/BF02586115.
[23] Höganäs, Material and powder properties. Höganäs Handb. Sintered Components, 2013, p. 86. https://www.hoganas.com/globalassets/media/sharepoint-documents/HandbooksAllDocuments/Handbook1Material_and_Powder_Properties_December_2013_0674HOGinteractive.pdf.
[24] L. Azouz, F. Dahmoune, F. Rezgui, C. G'Sell, Full factorial design optimization of anti-inflammatory drug release by PCL–PEG–PCL microspheres, Mater. Sci. Eng. C 58 (2016) 412–419, https://doi.org/10.1016/j.msec.2015.08.058.
[25] G. Dutta, D. Bose, Effect of sintering temperature on density, porosity and hardness of a powder metallurgy component, Int. J. Emerg. Technol. Adv. Eng. Website Www.Ijetae.Com. 2 (2012) 121–123.
[26] S. Kiranmayee Manchili, Role of Nanopowder as Sintering Aid in the Densification of Water Atomized Ferrous Powder, 2018.
[27] M. Dlapka, H. Danninger, C. Gierl, B. Lindqvist, Defining the pores in PM components, Met. Powder Rep. 65 (2010) 30–33, https://doi.org/10.1016/S0026-0657(10)70093-X.